*Interaction and Multiscale Mechanics, Vol. 5, No. 1 (2012) 75-90*
DOI: http://dx.doi.org/10.12989/imm.2012.5.1.075


# Coupled foot-shoe-ground interaction model to assess landing impact transfer characteristics to ground condition

S.H. Kim[1], J.R. Cho*[1,2], J.H. Choi[1], S.H. Ryu[1] and W.B. Jeong[1]

[1]*School of Mechanical Engineering, Pusan National University, Busan 609-735, Korea*
[2]*Research & Development Institute of Midas IT., Gyeonggi 463-400, Korea*

*(Received August 17, 2011, Revised February 27, 2012, Accepted March 3, 2012)*

**Abstract.** This paper investigates the effects of sports ground materials on the transfer characteristics of the landing impact force using a coupled foot-shoe-ground interaction model. The impact force resulting from the collision between the sports shoe and the ground is partially dissipated, but the remaining portion transfers to the human body via the lower extremity. However, since the landing impact force is strongly influenced by the sports ground material we consider four different sports grounds, asphalt, urethane, clay and wood. We use a fully coupled 3-D foot-shoe-ground interaction model and we construct the multi-layered composite ground models. Through the numerical simulation, the landing impact characteristics such as the ground reaction force (GRF), the acceleration transfer and the frequency response characteristics are investigated for four different sports grounds. It was found that the risk of injury, associated with the landing impact, was reduced as the ground material changes from asphalt to wood, from the fact that both the peak vertical acceleration and the central frequency monotonically decrease from asphalt to wood. As well, it was found that most of the impact acceleration and frequency was dissipated at the heel, then not much changed from the ankle to the knee.

**Keywords:** coupled foot-shoe-ground interaction model; landing impact force; ground condition; ground reaction force; acceleration transfer; frequency response.

## 1. Introduction

Occupying the large portion of the foot motions in most court sports, jumping and landing events may, but frequently, cause the various sports injuries and influence the game competency (Nigg 1986). Starting from the lower extremity motion initiated by the knee flexion, these events accompany a sequence of stretch and shortening motions of human knee and hips. Here, the final landing step inherently produces the impact force according to the collision between the human foot and the sports ground. The landing impact not only give rise to the direct shock to the foot but also transfers up to the human head via the lower extremity, even though it is partially dissipated by the inherent viscous damping of the human muscles, tissues and bones (Denoth 1986).

* Corresponding author, Vice director, E-mail: jrcho@pusan.ac.kr

The landing impact intensity is usually measured in terms of the ground reaction force (GRF), while its transfer through the human body is estimated by the acceleration and frequency responses. The landing impact characteristics, such as the peak impact force, the loading rate, the center of pressure as well as the above-mentioned three major quantities, are greatly influenced by the dynamic and external factors (Nigg 1986, Cavanagh 1990). As the dynamic factors which depend on the player's propensity and training, there exist the landing posture and the muscular activity. While, the external factors such as sports shoe and the ground material are independent of the player's will, so that their importance is increasing nowadays so as to protect various sports injuries and to improve the playing competency.

Regarding the studies on the effects of the external factors, traditionally the theoretical and experimental approaches have been widely adopted. Nigg and Liu (1999) proposed a mathematical model for analyzing the impact characteristics to the mid-sole hardness, while Shorten and Himmelsbach (2002) theoretically investigated the impact dissipation feature of sports ground using the Hertz contact theory. Meanwhile, Hennig and Lafortune (1991) performed the actual experiments to evaluate the ground reaction force and the tibia acceleration in running motion, and Tillman *et al*. (2002) measured the in-shoe plantar motions in running for various sports ground conditions.

More recently, however the use of numerical approach utilizing the finite element method is rapidly increasing thanks to the advances in the modeling and numerical analysis technologies as well as computation facilities. Bandak *et al*. (2001) constructed a 3-D finite element model of the human lower extremity considering major bones, ankles, ligaments and soft tissue of the plantar surface with the help of the medical CT images, in order to investigate the time histories of acceleration and force stemming from the landing impact. Asai and Murakami (2001) introduced a 3-D foot skeleton FEM model and numerically analyzed the foot skeleton-ground interaction in walking with a commercial FEM code. Later, Cheung *et al*. (2004) proposed an elaborate 3-D coupled FE foot model, in which soft tissue, bony and ligamentous structures are modeled using MRI images, and they investigated the barefoot-ground interaction characteristics. This coupled model was extended to numerically investigate the foot-sole-ground interaction (Dai *et al*. 2006, Cheung and Zhang 2008) and the foot-shoe-ground interaction (Cheung and Nigg 2007). Gefen (2002, 2003) and Wu (2007) constructed 2-D sectional FE foot models composed of bones, ligaments, cartilages and plantar fascia by utilizing MR and CT images, and they numerically analyzed the structural behavior of the diabetic foot during standing with a commercial FEM code. Cheng *et al*. (2008) and Garcia-Gonzalez *et al*. (2009) introduced a detailed 3-D foot model considering bones, cartilages, ligaments and plantar fascia and investigated the stretch effects on the plantar fascia and its stress and strain distributions.

The goal of the current study is to numerically investigate how the impact force at landing is dissipated by the lower extremity depending upon sports ground type, under the assumption that a human landing is the same on each ground type. To do this, the most important issue is how to model the foot-shoe and shoe-ground interactions, because the final numerical accuracy is absolutely dependent of the appropriateness of the numerical model constructed. In this context, the use of the 3-D coupled foot-shoe-ground interaction model is prerequisite for the reliable numerical investigation of the effects of the ground type. A 3-D coupled foot-shoe finite element model (Kim 2005, Cho *et al*. 2009a, 2009b) is used, in which not only the detailed geometry of foot and shoe is considered but also the interaction effects are fully reflected. And, four different sports grounds, asphalt, urethane, clay and wood are modeled by taking their complex material and structural

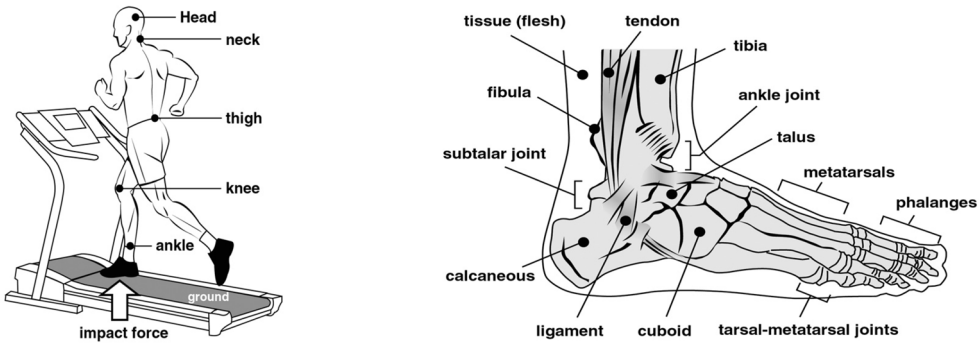


(a) (b)

Fig. 1 Representation: (a) landing impact force experiment and (b) foot and lower leg

composition into consideration. The variations of ground reaction force, acceleration transfer and frequency response to the sports ground material are examined.

## 2. Landing impact and sports ground

A collision between the foot and the ground inherently accompanies the impact force, as depicted in Fig. 1(a), which transfers up to head from foot through the human body. The landing impact is usually characterized by its peak and time history which are influenced by many factors such as the ground hardness, shoe and heel, the impact velocity $V$ and the landing posture, the effective human mass $m$, and the joint angle and the muscle pre-activation. Referring to a book by Nigg (1986), the peak impact $F_{\max}$ is calculated approximately by $F_{\max} = V\sqrt{km}$, where the spring constant $k$ is a function of the material properties of the ground-shoe-foot system and the kinematic conditions of joints, muscles, tendons and ligaments, particularly those of the lower extremity shown in Fig. 1(b).

The landing impact intensity is traditionally measured by the ground reaction force and the loading rate, while the impact force transfer through the human body is evaluated in terms of the acceleration and frequency responses at the major body parts such as heel, ankle, shank, knee, thigh, neck and head. As is given in the books by Nigg (1986) and Cavanagh (1990), the studies on the measurement, analysis and characteristic investigation of such quantities associated with the landing impact have been made by many investigators. Differing from these traditional studies based on experimental and theoretical methods, the most important considerations for the numerical approach which is widely adopted nowadays should be focused on the geometry and material modeling and the interaction between ground, shoe and foot. The reason is because the numerical analysis results are definitely affected by the appropriateness of the numerical model.

Referring to Fig. 1(b), the human foot is composed of a number of bones, cartilages, tendons and ligaments which are embedded into the underlying tissue in highly complicated composition structure. As a result, the construction of a detailed simulation model of the human foot becomes a painstaking task owing to the complex structure, the complicated joint motions and the nonlinear material behavior. However, in a biomechanics point of view, the relative motions of ankle, subtalar and tarsal-metatarsal joints, which are activated and controlled by muscles and tendons, are

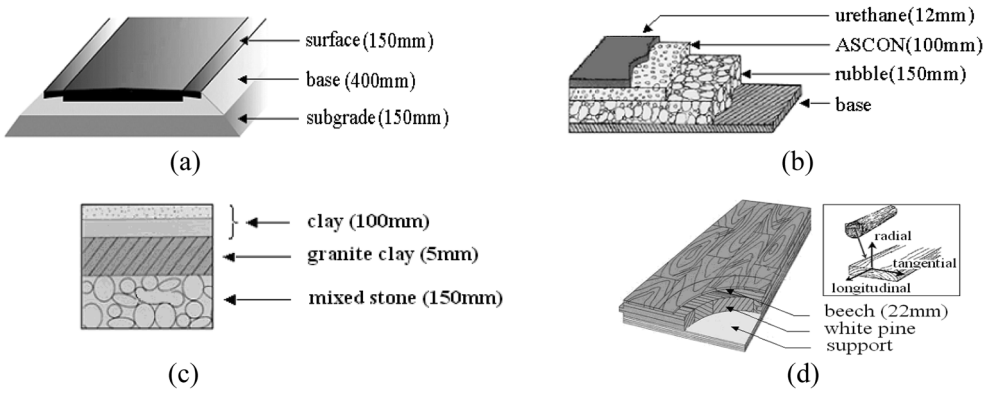


Fig. 2 Sports grounds: (a) asphalt, (b) urethane, (c) clay and (d) wood

important because such motions play a key role in describing the kinematics of the foot-leg skeleton system. Furthermore, soft tissue and ligaments characterize the shock dissipation and the impact force transfer through the human body.

Meanwhile almost all sports grounds are commonly in the lamination structure of several different material layers, as represented in Fig. 2. The material and structural compositions and the dimensions of each ground are dependent upon the type of sports game and standardized by the regulations of the corresponding international sports association. In general, sports grounds are classified largely into outdoor and indoor ones, and the major ground requirements against the environmental conditions are distinguished. However, the impact force and transfer characteristics are commonly influenced by the ground harness, regardless of the ground type. In this connection, the construction of sports ground models considering the detailed lamination structure and the accurate material behaviors becomes the most important step for the reliable numerical simulation.

## 3. 3-D coupled foot-shoe-ground model

A 3-D coupled foot-shoe finite element model (Kim 2005, Cho *et al*. 2009a, 2009b) used in this study is represented in Fig. 3(a), together with the schematic representation of its structural composition shown in Fig. 3(b). The most prominent feature of this state-of-the-art model is the realization of the in-shoe lower limb, so that any kind of foot motion that may be occurred in real sports games can be simulated with perfect freedom. Thus, a numerical simulation with this model does not rely on any kind of independent experimental data any longer. However, the drawback of this model is the simplification of foot skeleton, joints, tissue, ligaments and tendons. Both the skeleton and tissue geometries are approximately modeled with the help of shoe lasts and foot anatomic pictures. As depicted in Fig. 3(b), ankle and subtalar joints are modeled as a combined joint which is composed of a rigid ball, several ligament link and cartilage beam elements, so that foot and shoe are able to freely rotate with the appropriate rotational rigidity. The rigidity moduli chosen for the ligament and cartilage elements are recorded in Table 1 of Section 4, and their suitability has been through the preliminary comparison simulation.

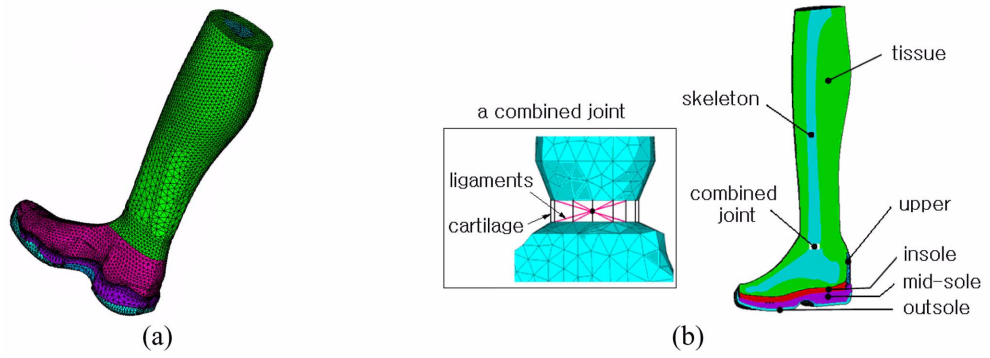


Fig. 3 3-D coupled foot-shoe model: (a) finite element model and (b) schematic representation

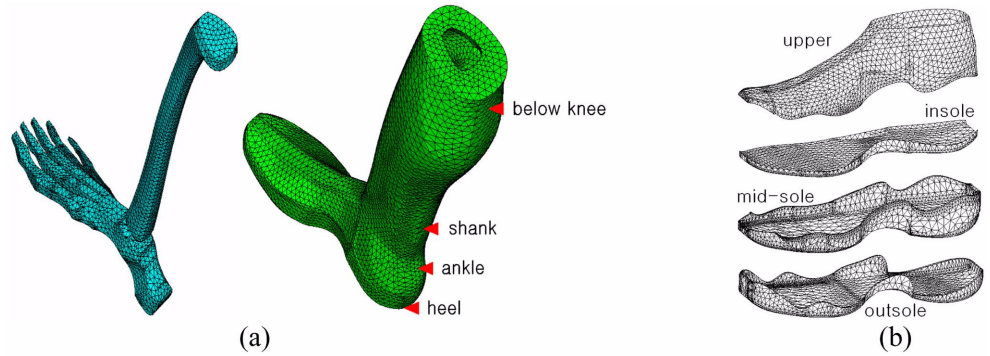


Fig. 4 Finite element models: (a) skeleton and soft tissue of lower extremity and (b) sport shoe parts

Fig. 4(a) represents the finite element models of the lower limb skeleton and the soft tissue, for which the mesh geometries are not constructed using the cadaver data but rather simply generated as mentioned above. It is worth to mention that this simple geometry modeling may lead to the inaccuracy in the vertical acceleration prediction owing to the wobbling mass effect (Nigg and Liu 1999), and the numerical accuracy of this simple model could be assessed by comparing with the elaborate MRI image-based model. The skeleton model constructed with 4-node tetrahedron elements is composed of two bone assemblies and a combined joint. Referring to Fig. 1(b), tibia and fibular are modeled as a single bone assembly while the other bones are modeled as another bone assembly, by neglecting the minor joints except for the ankle and subtalar joints. And, the soft tissue model is also generated with 4-node tetrahedron elements and its inner surface is carved such that the outer surface of the lower limb skeleton completely contacts with the tissue model. Both meshes are separately generated so that their mesh discretization patterns at the common interface are not compatible, requiring the surface-to-surface tying algorithm (Cho *et al*. 2004) to assemble these two incompatible meshes. Bones, tissue, ligaments and cartilages are assumed to be linearly isotropic and the detailed material properties are given in Table 1 given in Section 4.

Referring to Fig. 4(b), three soles are modeled with 4-node tetrahedron elements while upper is modeled with 3-node shell elements. Since outsole is manufactured with rubber-like materials, its hyperelastic behavior is modeled by the five-term Moonley-Rivlin material model with the strain

Table 1 Material properties and element numbers set for lower limb and sports shoe (except for the outsole)

| Components | Young's modulus $E$ ($MPa$) | Poisson's ratio $\nu$ | Mass density $\rho$ (kg / m$^3$) | Total element number |
|---|---|---|---|---|
| Bone | 7,500 | 0.34 | 1,500 | 21,656 |
| Tissue | 1.15 | 0.49 | 9,500 | 82,578 |
| Ligament (links) | 11.5 | 0.34 | – | 37 |
| Cartilage (beams) | 10.0 | 0.34 | – | 6 |
| Upper | 11.76 | 0.35 | 9,400 | 2,865 |
| Insole | 1.98 | 0.35 | 2,300 | 4,797 |
| Mid-sole | 2.49 | 0.35 | 2,300 | 19,997 |

energy density functional $W$ defined by

$$W(I_i) = C_{10}(I_1-3) + C_{01}(I_2-3) + C_{11}(I_1-3)(I_2-3) + C_{20}(I_1-3)^2 + C_{30}(I_3-3)^3 + \frac{1}{2\kappa}(I_3-1)^2 \tag{1}$$

with $I_i$ being the invariants of Green-Lagrange strain tensor. Note that the material constants $C_{ij}$ are determined by the least-square fitting of experimental data and the bulk $\kappa$ is introduced to enforce the incompressibility of rubber. And, the Blatz-Ko form model (Blatz and Ko 1962) is employed to describe the elastic behaviors of mid-sole and insole which are manufactured with polyurethane-like materials. The corresponding strain energy density functional $W$ is given by

$$W(I_1, I_2, I_3) = \frac{G}{2}\left(\frac{I_2}{I_3} + 2\sqrt{I_3} - 5\right) \tag{2}$$

The detailed material properties of four shoe parts are recorded in Table 1. Each shoe part is completely bonded to its neighbor parts node-by-node, because finite element meshes of each shoe part are generated such that the mesh distributions of two adjacent parts are exactly same at the common interfaces. Meanwhile, the shoe model is assembled such that its inner surface can be appropriately contacted with the outer surface of the soft tissue model as in the real contact between the both surfaces. The interaction between foot and shoe is implemented by employing the frictional surface-to-surface contact with the frictional coefficient $\mu$ of 0.5 (Dai *et al*. 2006).

Fig. 5 represents the finite element models of four different sports grounds which are generated with 8-node cubic elements. The detailed material properties of each material layer in four ground models are recorded in Table 2. In case of the asphalt ground, asphalt, base and subgrade layers are discretized into three, four and two in the thickness direction respectively, and all the three material layers are assumed to be linearly isotropic. Meanwhile, rubble and base layers in the urethane ground are modeled as a homogenized base layer by the linear rule of mixtures (Cho and Oden 2000) with the equal volume fraction ratios, and the resulting three material layers are assumed to be linear isotropic and discretized into one, three and two in the thickness direction respectively. In the similar manner, clay and granite clay layers in the clay ground are combined into a clay layer, and the resulting two material layers are modeled as a homogenized linear isotropic layer by the linear rule of mixtures and discretized into four and two in the thickness direction respectively. Meanwhile, beech panel in the wood ground is modeled as orthotropic, by assuming white pine to be isotropic and by excluding the support layer in the FEM modeling. Beech panel and white pine

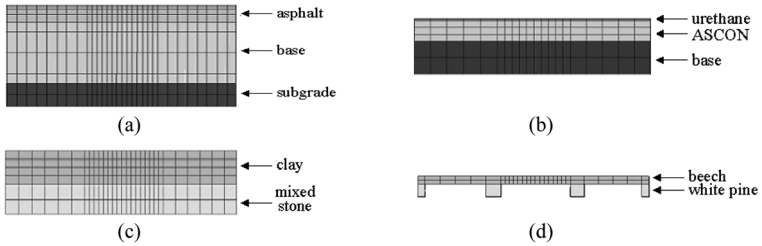


Fig. 5 Section view of FEM models of sports grounds: (a) asphalt, (b) urethane, (c) clay and (d) wood

Table 2 Material properties of sports grounds (except for the wood ground) (Chou and Bobet 2002, Medvedev and Orgel 1990, Timm and Priest 2006)

| Item | Asphalt | | | Urethane | | | Clay | |
|---|---|---|---|---|---|---|---|---|
| | Asphalt | Base | Subgrade | Urethane | ASCON | Rubble | Clay | Mixed stone |
| Young's modulus $E$ ($MPa$) | 10,500 | 300 | 100 | 4.8 | 10,000 | 15,000 | 10 | 20,000 |
| Poisson's ratio $\nu$ | 0.35 | 0.35 | 0.35 | 0.4 | 0.3 | 0.3 | 0.36 | 0.3 |

are discretized into two and one in the thickness direction respectively. In order to secure the numerical simulation accuracy, the ground region where sports shoe will be contacted is locally refined in both planar and thickness directions (see also Fig. 6). The total element numbers are as follows: $270 \times 270$ for the asphalt, $120 \times 120$ for the urethane, $180 \times 180$ for the clay and $60 \times 60$ for the wood ground model, respectively.

## 4. Numerical simulation

The vertical straight landing event of a human foot from $h = 300$ mm above the ground with the zero initial velocity is taken. For the comparison purpose, we assume that a human landing is the same on each ground type, even though a human will adapt their landing based on the ground and shoe types. The total weight of the human body is set by 60 kgf and its dynamic effect is reflected by lumping the total body mass to the mass center of the foot-shoe coupled model, as depicted in Fig. 6. In order to shorten the total CPU time, the landing duration only from the vertical position of 5 mm above the ground is simulated, by specifying the initial velocity $V_{ini} = \sqrt{2gh} = 2.405$ m/$s$ to the entire foot-shoe coupled model. The frictional dynamic contact analysis was carried out by ANSYS (2005), for which the frictional coefficient $\mu$ between the outsole and the ground and the penalty parameter $k_p$ for constraining the material incompressibility are set by 0.5 (Cho *et al*. 2005) and 10MPa respectively. Note that the frictional coefficients are set equally for the four ground conditions because the main observation of the current study focuses on the behavior of both shoe and foot in the direction normal to the ground. The mesh density was chosen based the model evaluation given in Section 4.1, and the time step size was set by $\Delta t \le 2/\omega_{\max}$ ($\omega_{\max}$ ~ the largest element frequency) for securing the numerical convergence and stability (Cho *et al*. 2005).

The material properties and the total element numbers set for each shoe part, except for the

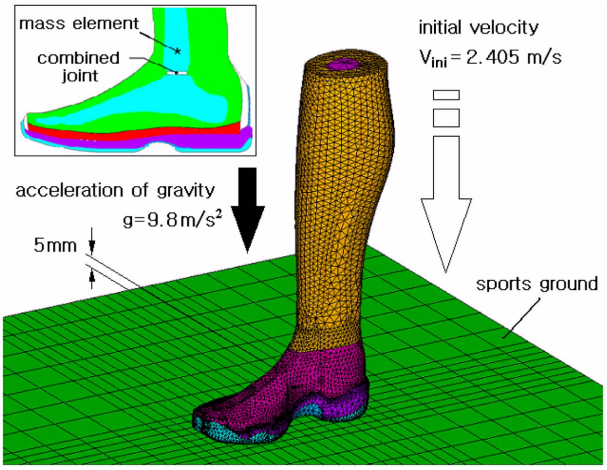


Fig. 6 Loading and boundary conditions for the landing impact simulation

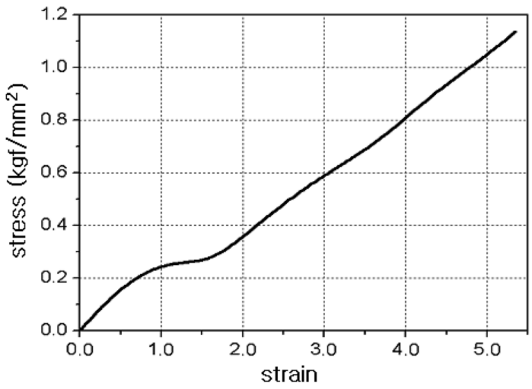


Fig. 7 Stress-strain curve of the outsole obtained by uni-axial tension test

outsole, are recorded in Table 1. Note that the material properties of bone, tissue, ligament and cartilage were chosen by referring to Dai *et al*. (2006) and Yamada (1970), while the others were determined by the uni-axial tension test of individual shoe part specimens. Fig. 7 shows the stress-strain curve of outsole material which was obtained by the uni-axial tension test at Korea Institute of Footwear & Leather Technology, from which five Moonley-Rivlin constants are determined as follows: $C_{10} = -0.00149$, $C_{01} = 0.11732$, $C_{11} = -0.00182$, $C_{20} = 0.01720$ and $C_{30} = 0.02$ respectively. The outsole is discretized with 6,574 4-node tetrahedron elements. Note that the soft tissue is assumed to be passive such that it does not depend upon muscle activation level.

Four sports grounds are non-uniformly discretized with the total of 3,600-72,900 elements, depending on the ground type. As the boundary condition, the entire bottom surfaces of each sports ground model are fixed. The material properties of isotropic material layers of three sports grounds are given in Table 2. The Young's modulus and Poisson's ratio of white pine in the wood ground are set by $E = 10{,}000$ MPa and $\nu = 0.3$, while nine orthotropic material constants of beech are set as follows: $E_x = 10{,}000$ MPa, $E_y = E_z = 600$ MPa, $\nu_{yz} = 0.35$, $\nu_{xy} = \nu_{xz} = 0.2$, $G_{yz} = 710$ MPa and $G_{xy} = G_{xz} = 810$ MPa respectively (Tabiel and Wu 2006).

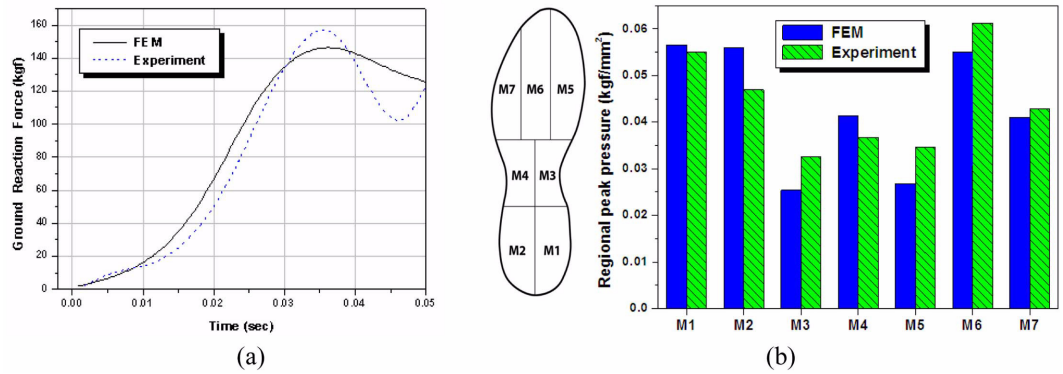


(a) (b)

Fig. 8 Comparison with experiments: (a) time history of GRF and (b) regional peak pressures

### *4.1 Model evaluation*

The landing simulation was carried out up to 0.05 sec from the initial contact of outsole with the clay ground. In order to evaluate the simulation model, the actual experiment was also carried out with ten subjects composed of five males and five females. The ages, heights and weights of the subjects are $23.2 \pm 2.90$ years, $169.0 \pm 7.15$ cm and $60.4 \pm 13.06$ kgf. Fig. 8(a) compares the time histories of the ground reaction force (GRF) between the numerical simulation and the actual experiment. The curve indicated by experiment is the averaged value of the GRF time histories of ten subjects which were measured by AMTI force platform (Cavanagh 1990, Tabiel and Wu 2000). The numerical simulation parameters, such as the body weight, the landing height and the ground stiffness and the friction coefficient were adjusted to the experimental conditions. As a whole, the numerical prediction is in a good agreement with the experiment such that the peak value occurs at almost the same time $t = 0.036$ sec. One noticeable difference is that the numerical prediction can not successfully capture the oscillation after the peak, it is because the inherent viscous damping of soft tissue and sports shoe is not considered in the numerical analysis. We assume that the damping effects are the same for the comparative investigation of the landing impact transfer characteristics to the ground type. The peak value of 148 kgf corresponds to 2.7 times of the total body weight (BW), which is consistent with the report by Mann and Hagy (1980) that the relative peak GRF with respect to the total body weight reaches generally 2-3 BW.

Fig. 8(b) depicts the seven sub-regions of the outsole which are conventionally used to evaluate the regional peak pressures resulting from the collision between the outsole and the ground. The experimental results were obtained by the traditional EMED test. The experiment was carried out with the ten subjects chosen for the previous GRF experiment and the experimental data of ten subjects were averaged. The comparison confirms that the present coupled foot-shoe model produces the acceptable numerical accuracy with the maximum relative error equal to 28.2%. One noticeable fact is that the numerical simulation overestimates the peak pressure in the rear-foot region but underestimates in the fore-foot regions, which is caused by the limitation in the modeling of ankle and subtalar joints and in modulating the rotational stiffness of the combined joint.

The points indicated by + in the right plot of Fig. 9 represent the locus of the center of pressure exerted on the insole during the entire landing event. The locus was obtained by the numerical simulation. With the nodal pressure values $p_i$ at each finite element node $(x_i, y_i)$, the center of

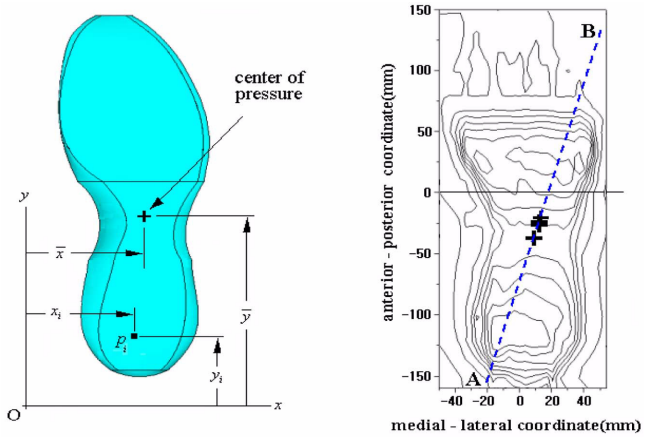


Fig. 9 Movement of the center of pressure during the landing motion

pressure $(\bar{x}, \bar{y})$ is calculated by

$$\bar{x} = \sum p_i x_i / \sum p_i, \qquad \bar{y} = \sum p_i y_i / \sum p_i \tag{3}$$

The dotted line connecting two points $A$ and $B$ indicates the reference line for evaluating the movement of the center of pressure. In other words, the landing instability and over-pronation do not occur when the center of pressure moves along this reference line. From the numerical results, we found that the deviation of the center of pressure from the reference line is negligible, not leading to undesired injury caused by the over-pronation. The detailed maximum deviation from the reference line $A$-$B$ is found to be 3.49 mm in the medial-lateral direction and 14.30 mm in the anterior-posterior direction.

### 4.2 Results and discussion

We next carried out the numerical simulations for four different ground types to investigate the variations of ground reaction force, acceleration transfer and frequency response. The ground reaction forces (GRFs) exerted on the outsole for four different sports grounds are compared in Fig. 10(a). The asphalt ground produces the highest peak GRF while the wood ground does the lowest value, and asphalt, urethane and clay grounds do not show the remarkable difference when compared with the wood ground. It is because the vertical stiffness of the wood ground is much smaller than other three sports grounds due to its structural composition characteristic, even though white pine and beech are stiff materials. The slopes of the GRF time histories which are called the loading rates of the impact force are compared in Fig. 10(b), where the dependence of the peak values on the ground type shows the same trend as the GRF.

The detailed peak values of the contact pressure, impact force and loading rate which are evaluated at the outsole are recorded in Table 3. Since both the peak value and its location vary with the time, the values given in Table 3 were extracted from all the pressure values at the Gaussian integration points throughout the entire time period of observation. The peak GRF is ranged from 2.3 to 3.17 BW, which is consistent well with the experimental data reported by Mann

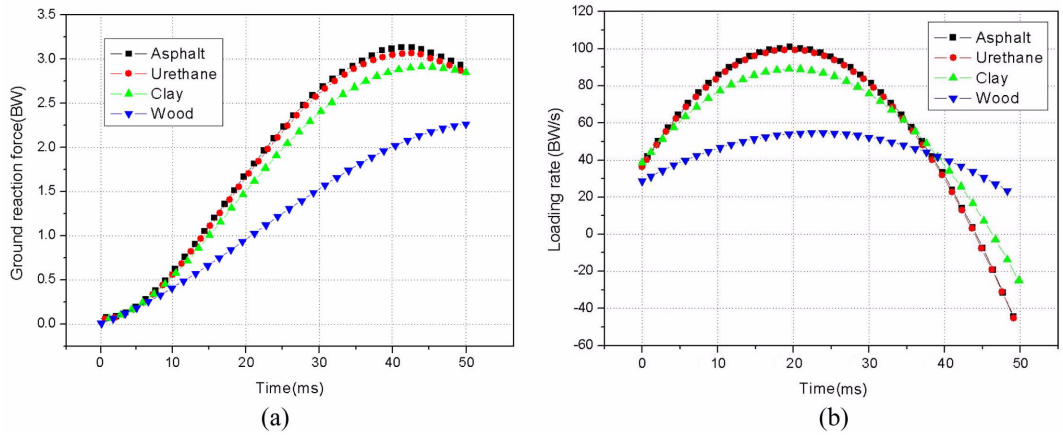


Fig. 10 Time histories: (a) ground reaction force (GRF) and (b) loading rate

Table 3 Peak values in the impact force transfer to the ground material

| Item | Asphalt | Urethane | Clay | Wood |
|---|---|---|---|---|
| Peak pressure (kgf / mm$^2$) | 0.059 | 0.055 | 0.052 | 0.042 |
| Peak impact force (BW) | 3.2 | 3.1 | 2.8 | 2.3 |
| Peak loading rate (BW/*s*) | 101.4 | 100.6 | 89.8 | 57.8 |

and Hagy (1980) that the peak GRF reaches 2-3 BW. Meanwhile, the peak loading rate in the current vertical landing event is ranged from 57.8 to 101.4 BW/*s*.

Time histories of the vertical acceleration which were evaluated at four different positions of the foot-leg model are represented in Fig. 11. In the real kinesiology experiments, accelerometer sensors are attached to the skin of human body, so that the numerical results were taken from the finite element nodes corresponding to the measuring points on the outer skin surface, as represented in Fig. 4(a). At the heel position, the vertical acceleration shows the typical transient-dominated response and does not show the remarkable dependence on the ground material. However, the transient behavior in the vertical acceleration response remarkably disappears and the influence of the ground material becomes clear, as the evaluation point goes far from the impact position. In the same pattern as the previous reaction force, the wood ground exhibits the quite distinct time response with the lowest magnitude, when compared with the remaining three sports grounds.

As given in Table 4, the peak vertical acceleration shows the uniform decrease from heel to ankle and from shank to below the knee, regardless of the ground material. However, the vertical acceleration response produces the negligible change in its peak value from ankle to shank, except for the remarkable reduction of the transient and oscillatory behavior. Thus, the impact transfer through the lower extremity is characterized as follows: the significant reduction in both the peak acceleration and the transient behavior from heel to ankle, the remarkable reduction in both the transient behavior and the oscillation from ankle to shank, and the additional reduction in the peak acceleration from shank to below the knee. Note that this impact transfer characteristics may become different depending on the landing posture with different knee angles. The knee angle influences the effective mass of the lower extremity such that the effective mass decreases in

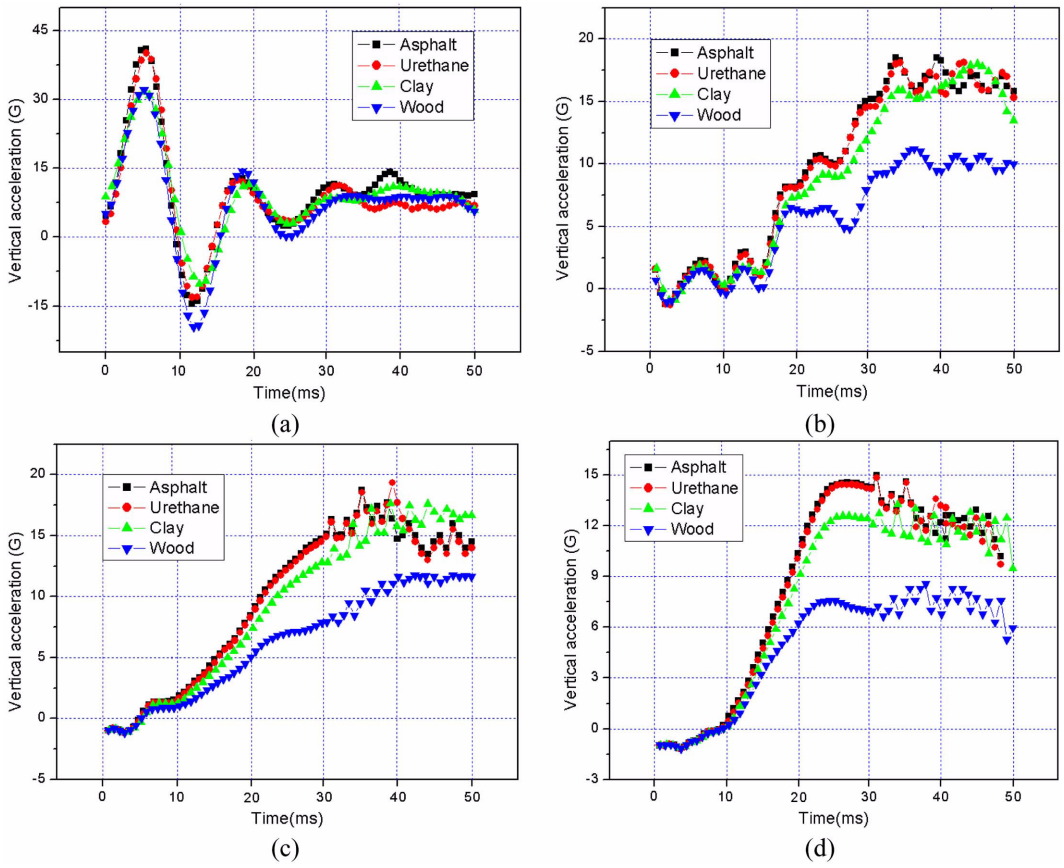


Fig. 11 Time histories of the vertical acceleration: (a) heel, (b) ankle, (c) shank and (d) below knee

Table 4 Peak vertical accelerations at four evaluation positions for four different sports grounds (unit: *G*)

| Location | Asphalt | Urethane | Clay | Wood |
|---|---|---|---|---|
| Heel | 41.3 | 40.2 | 32.2 | 31.1 |
| Ankle | 18.5 | 18.1 | 17.9 | 11.1 |
| Shank | 18.7 | 19.4 | 15.5 | 11.7 |
| Below knee | 15.0 | 14.9 | 13.3 | 8.4 |

proportional to the decrease of the knee angle (Nigg 1986, Denoth 1986, Nigg and Liu 1999). Thus, the impact peaks and the peak amplitudes which are presented in this paper for the straight vertical landing would be smaller for non-straight landing events. Even though the straight vertical landing posture is not frequent in court sports, it plays an important role in service and smashing motions in tennis, shooting and rebound motions in basketball, and broking motion in volleyball.

The frequency responses at four different evaluation positions are represented in Fig. 12. Heel shows the wide frequency band with the relatively high central frequency. However, both the center frequency and the frequency band are shown to be gradually reduced as the evaluation position goes far from the impact location. This trend is consistent with the previous acceleration response,

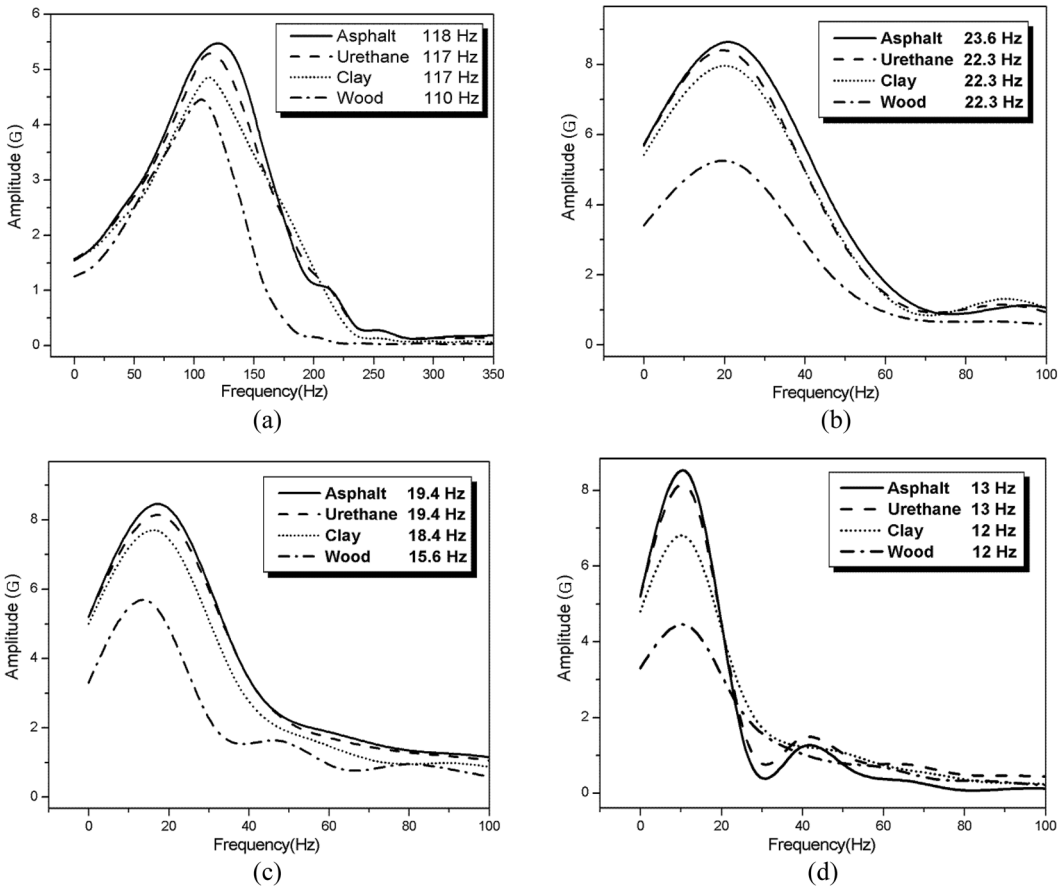


Fig. 12 Frequency response: (a) heel, (b) ankle, (c) shank and (d) below knee

Table 5 The central frequencies at four positions to the ground material (unit: *Hz*)

| Location | Asphalt | Urethane | Clay | Wood |
|---|---|---|---|---|
| Heel | 118.0 (5.59) | 117.0 (5.45) | 117.0 (4.98) | 110.0 (4.69) |
| Ankle | 23.6 (8.57) | 22.3 (8.33) | 22.3 (7.92) | 22.3 (5.20) |
| Shank | 19.4 (8.38) | 19.4 (8.07) | 18.4 (7.62) | 15.6 (5.61) |
| Below knee | 13.0 (8.20) | 13.0 (7.86) | 12.0 (6.71) | 12.0 (4.41) |

* The numerical values in ( ) indicate the amplitudes (unit: *G*).

confirming that the initial high-frequency transient response caused by the landing impact is remarkably dissipated by the human foot and leg. Regarding the ground material, the prominent influence is observed from the amplitude such that the peak amplitude shows the uniform decrease from asphalt to wood for all the evaluation positions. The influence on the central frequency and the frequency band is not shown to be significant. As a result, one can infer that the damage stemming from the landing impact becomes weaker as the ground material changes from asphalt to wood. Table 5 summarizes the variations of the central frequency and the amplitude to the ground type and

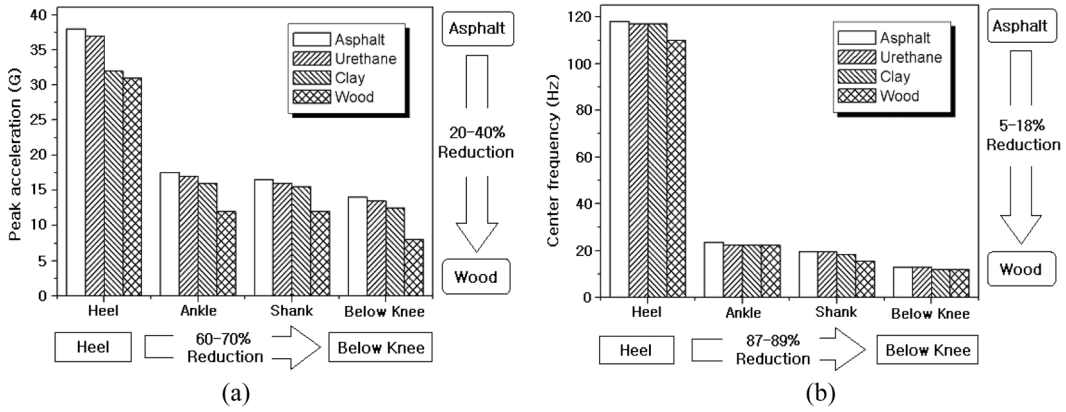


Fig. 13 Comparison: (a) peak acceleration and (b) central frequency

the evaluation position.

The reductions in the peak acceleration and the central frequency through the lower extremity are schematically summarized in Fig. 13, for four different sports grounds. With respect to the evaluation position, the peak acceleration and the central frequency are reduced respectively by 60-70% and 87-89% from heel to below the knee. Thus, most of the impact acceleration and frequency is dissipated at the heel. Meanwhile, the reductions in the both quantities from asphalt to wood reach 20-40% and 5-18% respectively. Thus, the influence of the ground condition on the landing impact transfer through the lower extremity is significant, particularly from heel to ankle.

## 5. Conclusions

The landing impact transfer characteristics of in-shoe human foot through the lower extremity have been investigated with respect to the ground type. The foot-shoe and shoe-ground interactions were fully reflected by using the 3-D coupled foot-shoe-ground finite element model. The numerical experiments show that the impact transfer characteristics can be classified into three regions; the significant reduction in the peak acceleration and transient behavior from heel to ankle, the remarkable reduction in both the transient oscillation from ankle to shank and the additional reduction in the peak acceleration from shank to below the knee. The high-frequency transient impact response with the large amplitude is dissipated by the lower extremity such that 60-70% reduction in the peak acceleration and 87-89% reduction in the central frequency from heel to below the knee, depending on the ground condition.

The ground condition exhibits the remarkable influence on the magnitudes in the ground reaction force, loading rate, vertical acceleration and frequency responses. However, the influence on the central frequency and the frequency band is negligible. The wood ground produces the lowest peak values in the above-mentioned four responses owing to its structural composition characteristic, but the difference among asphalt, urethane and clay are not significant. The reductions in the peak acceleration and the central frequency from asphalt to wood are 20-40% and 5-18%, respectively. This concludes that the damage stemming from the landing impact becomes weaker as the ground material changes from asphalt to wood.

The current study was made with the simple foot bone model by neglecting the damping effect of soft tissue and shoes under the assumption that a human landing is the same on each ground type. To overcome the assumption and limitation of the current study, the landing simulation with the elaborate MRI-based FEM model by considering the different landing postures to the ground and shoe types and the damping effect of soft tissue and shoe deserves future work.

## References


Ansys Inc. (2005), *ANSYS User's Manual*, Ver. 5.3.

Asai, T. and Murakami, H. (2001), "Development and evaluation of a finite element foot model", *Proc. of the 5th Symposium on Footwear Biomechanics (Eds. E.M. Hennig, A. Stacoff)*, Zuerich, 10-11.

Bandak, F.A., Tannous, R.E. and Toridis, T. (2001), "On the development of an osseo-ligamentous finite element model of the human ankle joint", *Int. J. Solids Struct*., **38**(10-13), 1681-1697.

Blatz, P.J. and Ko, W.L. (1962), "Application of finite element theory to the deformation of rubbery materials", *Trans. Soc. Rheol*., **6**, 223-251.

Cavanagh, P.R. (1990), *Biomechanics of distance running*, Human Kinetics Books, Champaign, IL.

Cheng, H.Y.K., Lin, C.L., Wang, H.W. and Chou, S.W. (2008), "Finite element analysis of plantar fascia under stretch-the relative contribution of windlass mechanism and Achilles tendon force", *J. Biomech*., **41**(9), 1937-1944.

Cheung, J.T.M. and Nigg, B.M. (2007), "Clinical applications of computational simulation of foot and ankle", *Sportorthopdie Sporttraumatologie*, **23**(4), 264-271.

Cheung, J.T.M. and Zhang, M. (2008), "Parametric design of pressure-relieving foot orthosis using statisticsbased finite element method", *Med. Eng. Phys*., **30**(3), 269-277.

Cheung, J.T., Zhang, M. and An, K.N. (2004), "Effects of plantar fascia stiffness on the biomechanical response of the ankle-foot complex", *Clin. Biomech*., **19**(8), 839-846.

Cho, J.R., Kim, K.W., Yoo, W.S. and Hong, S.I. (2004), "Mesh generation considering detailed tread blocks for reliable 3D tire analysis", *Adv. Eng. Softw*., **35**(2), 105-113.

Cho, J.R. and Oden, J.T. (2000), "Functionally graded material: a parametric study on thermal-stress characteristics using the Crank-Nicolson-Galerkin scheme", *Comput. Meth. Appl. Mech. Engrg*., **188**(1-3), 17-38.

Cho, J.R. and Park, S.B. (2009a), "Finite element landing impact simulation using a 3-D coupled foot shoe model", *Foot. Sci*., **1**(1), 97-98.

Cho, J.R., Park, S.B., Ryu, S.H., Kim, S.H. and Lee, S.B. (2009b), "Landing impact analysis of sports shoes using 3-D coupled foot-shoe finite element model", *J. Mech. Sci. Technol*., **23**(10), 2583-2591.

Cho, J.R., Shin, S.W. and Yoo, W.S. (2005), "Crown shape optimization for enhancing tire wear performance by ANN", *Comput. Struct*., **83**(12-13), 920-933.

Chou, W.I. and Bobet, A. (2002), "Predictions of ground deformations in shallow tunnels in clay", *Tunn. Undergr. Sp. Tech*., **17**(1), 3-19.

Dai, X.Q., Zhang, M. and Cheung, J.T.M. (2006), "Effect of sock on biomechanical responses of foot during walking", *Clin. Biomech.*, **21**(3), 314-321.

Denoth, J. (1986), "Load on the locomotor system and modeling", *Biomech. Running Shoes (Eds. B. Nigg)*, Human Kinetics Publisher, Champaign, 63-116.

Garcia-Gonzalez, A., Bayod, J., Prados-Frutos, J.C., Losa-Iglesias, M., Jules, K.T., Bengoa-Vallejo, R.B. and Doblare, M. (2009), "Finite-element simulation of flexor digitorum longus of flexor digitorum brevis tendon transfer for the treatment of claw toe deformity", *J. Biomech*., **42**(11), 1697-1704.

Gefen, A. (2002), "Stress analysis of the standing foot following surgical plantar fascia release", *J. Biomech.*, **35**(5), 629-637.

Gefen, A. (2003), "Plantar soft tissue loading under the medical metatarsals in the standing diabetic foot", *Med. Eng. Phys*., **25**(6), 491-499.

Henning, E.M. and Lafortune, M.A. (1991), "Relationships between ground reaction force and tibial bone

acceleration parameters", *J. Sport Biomech*., **7**(3), 303-309.
Kim, S.H. (2005), "Evaluation of landing impact characteristics of court sports shoes by finite element method", *Master's Thesis*, Pusan National University, Korea.
Mann, R.A. and Hagy, J. (1980), "Biomechanics of walking, running and sprinting", *Am. J. Sport. Med*., **8**(5), 345-350.
Medvedev, V.P. and Orgel, A.M. (1990), "Some features of the interaction of the human locomotor apparatus with an elasticoplastic base", *Mech. Compos. Mater.*, **26**(1), 117-123.
Nigg, B.M. (1986), *Biomechanics of running shoes*, Human Kinetics Publisher, Champaign, IL.
Nigg, B.M. and Liu, W. (1999), "The effect of muscle stiffness and damping on simulated impact force peaks during running", *J. Biomech*., **32**(8), 849-856.
Shorten, M.R. and Himmelsbach, J.A. (2002), "Shock attenuation of sports surfaces", *Sport. Eng*., **4**, 152-158.
Tabiei, A. and Wu, J. (2000), "Three-dimensional nonlinear orthotropic finite element model for wood", *Compos. Struct*., **50**(2), 143-149.
Tillman, M.D., Fiolkwski, P., Bauer, J.A. and Reisinger, K.D. (2002), "In-shoe plantar measurements during running on different surfaces-changes in temporal and kinetic parameters", *Sport. Eng*., **5**(3), 121-128.
Timm, D.H. and Priest, A.L. (2006), "Material properties of the 2003 NCAT test track structural study", *NCAT Report 06-01*, Auburn University, Alabama.
Wu, L. (2007), "Nonlinear finite element analysis for musculoskeletal biomechanics of medial and lateral plantar longitudinal arch of virtual Chinese human after plantar ligamentous structure failures", *Clin. Biomech*., **22**(2), 221-229.
Yamada, H. (1970), *Strength of biological materials*, Williams & Wilkins, Baltimore, USA.